Schweizerischer Erdbebendienst
Service Sismologique Suisse
Servizio Sismico Svizzero
Servizi da Terratrembels Svizzer

ETH
Eidgenössische Technische Hochschule Zürich
Swiss Federal Institute of Technology Zurich

Solothurn - Zeughausplatz (SOLZ)

SITE CHARACTERIZATION REPORT

Clotaire MICHEL, Carlo CAUZZI, Daniel ROTEN

Valerio POGGI, Jan BURJANEK, Donat FÄH

Sonneggstrasse 5 CH-8092 Zürich Switzerland; E-mail: clotaire.michel@sed.ethz.ch

Last modified : November 5, 2013

Abstract

The station SOLZ of the Swiss Strong Motion Network located in the old city-centre of Solothurn, on deep moraine deposits, was newly installed in 2012. In order to characterize the velocity profile under the station, array measurements were performed in the city. We found first $10\,\mathrm{m}$ of under-consolidated moraine with a relatively low velocity around $250-400\,\mathrm{m/s}$ and a homogenous layer of moraine down to $80\,\mathrm{m}$ depth with a velocity of $500-700\,\mathrm{m/s}$. The Molasse rock, located below, has velocities around $800-1000\,\mathrm{m/s}$. The interface responsible for the fundamental resonance frequency at $1.45\,\mathrm{Hz}$ is located at $170\,\mathrm{m}$ depth. The velocity of the bedrock, which could be the Mesozoic basement is found around $1700\,\mathrm{m/s}$. $V_{s,30}$ is found to be close to $430\,\mathrm{m/s}$. The profile corresponds to ground type B in EC8 and E in SIA261. The theoretical SH transfer function and impedance contrast of the quarter-wavelength velocity computed from the inverted profiles show an amplification up to 4 for frequencies above $1.4\,\mathrm{Hz}$.

Contents

1 Introduction

The station SOLZ (Solothurn Zeughausplatz) is part of the Swiss Strong Motion Network (SSMNet) on the Swiss Plateau. SOLZ is a new site installed in the framework of the SSMNet Renewal project in 2012. This project includes also the site characterization. Passive array measurement has been selected as a standard tool to investigate these sites. Such a measurement campaign was performed on 15th March 2012 around the Zeughausplatz in the old town of Solothurn (Fig. 1), with a centre $10\,\mathrm{m}$ NE from the station SOLZ, in order to characterize the sediments under this station. According to the geological map, this station is located on moraine (Würm). This report presents the measurement setup, the results of the H/V analysis and of the array processing of the surface waves (dispersion curves). Then, an inversion of these results for a velocity profile is performed. Standard parameters are derived to evaluate the amplification at this site.

Canton	City	Location	Station code	Site type	Slope
Solothurn	Solothurn	Zeughaus	SOLZ	Moraine sediments	Slight slope

Table 1: Main characteristics of the study-site.

Figure 1: Picture of the site.

2 Experiment description

2.1 Ambient Vibrations

The ground surface is permanently subjected to ambient vibrations due to:

- natural sources (ocean and large-scale atmospheric phenomena) below $1\,\mathrm{Hz}$,
- local meteorological conditions (wind and rain) at frequencies around $1\,\mathrm{Hz}$,
- human activities (industrial machines, traffic…) at frequencies above $1\,\mathrm{Hz}$ [Bonnefoy-Claudet et al., 2006].

The objective of the measurements is to record these ambient vibrations and to use their propagation properties to infer the underground structure. First, the polarization of the recorded waves (H/V ratio) is used to derive the resonance frequencies of the soil column. Second, the arrival time delays at many different stations are used to derive the velocity of surface waves at different frequencies (dispersion). The information (H/V, dispersion curves) is then used to derive the properties of the soil column using an inversion process.

2.2 Equipment

For these measurements 12 Quanterra Q330 dataloggers named NR01 to NR12 and 14 Lennartz 3C 5 s seismometers were available (see Tab. 2). Each datalogger can record on 2 ports A (channels EH1, EH2, EH3 for Z, N, E directions) and B (channels EH4, EH5, EH6 for Z, N, E directions). The time synchronization was ensured by GPS. The sensor are placed on a metal tripod directly on the ground. Some points were located on the grass: a hole was dug to ensure a better coupling.

Digitizer	**Model**	**Number**	**Resolution**
	Quanterra Q330	12	$24\,\mathrm{bits}$
Sensor type	**Model**	**Number**	**Cut-off frequency**
Velocimeter	Lennartz 3C	14	$0.2\,\mathrm{Hz}$

Table 2: Equipment used.

2.3 Geometry of the arrays

Two array configurations were used, for a total of 4 rings of 10, 20, 50 and $100\,\mathrm{m}$ radius around a central station. The first configuration includes the 3 inner rings with 14 sensors; the second configuration includes the 2 outer rings plus 2 remaining stations of the first ring with 13 sensors. The minimum inter-station distance and the aperture are therefore 10 and $100\,\mathrm{m}$ and 10 and $200\,\mathrm{m}$, respectively. The experimental setup is displayed in Fig. 2. The final usable datasets are detailed in section 3.2.

Figure 2: Geometry of the arrays.

2.4 Positioning of the stations

The sensor coordinates were measured using a differential GPS device (Leica Viva), including only a rover station and using the Real Time Kinematic technique provided by Swisstopo. It allows an absolute positioning with an accuracy of about $3\,\mathrm{cm}$ on the Swissgrid. This accuracy could not be reached at points SOZ202, SOZ203, SOZ305, SOZ402, SOZ405 with accuracies of respectively $38, 22, 21, 17$ and $28\,\mathrm{cm}$), due to the surrounding buildings. These values remain however reasonable for array processing. However, the accuracy of points SOZ301 and SOZ401, located in a very narrow street was found to be 2.8 and $2.6\,\mathrm{m}$, respectively. Coordinates of point SOZ401 were extracted from the Swissimage, whereas coordinates of SOZ301 were found to be realistic. The same happened for point SOZ403 ($1.1\,\mathrm{m}$ accuracy) but its positioning could not be improved.

3 Data quality

3.1 Usable data

The largest time windows were extracted, for which all the sensors of the array were in position and the GPS synchronization was ensured. An unexplained problem of the Baler of station NR08 induced large gaps in the data (point SOZ103). This point is therefore not present in dataset 1 (nor in dataset 2), but only available as a shorter recording for H/V computation only. GPS measurement were not performed during the datasets to avoid additional disturbances. A very limited number of vehicles crossed the array (vehicles prohibited in the afternoon). However a construction site was actively working (pneumatic drill) between SOZ304 and SOZ403 and can clearly be seen on the time histories until 14:50. A noticeable peak can be seen on all recordings at $1.05\,\mathrm{Hz}$ and may affect the results. In dataset 1, point SOZ301 shows particularly high noise in all components without clear explanation for it. Points SOZ304 is clearly affected by the pneumatic drill. Moreover, point SOZ102 shows abnormally high amplitudes, maybe due to bad coupling. The characteristics of the datasets are detailed in Tab. 3.

3.2 Data processing

The data were first converted to SAC format including in the header the coordinates of the point (CH1903 system), the recording component and a name related to the position. The name is made of 3 letters characterizing the location (SOZ here), 1 digit for the ring and 2 more digits for the number in the ring. The response of the sensor was not corrected and the values (in counts) were not converted to $\mathrm{m/s}$.

Dataset	Starting Date	Time	Length	F_s	Min. inter-distance	Aperture	# of points
1	2012/03/15	11:41	119 min	200 Hz	10 m	100 m	13
2	2012/03/15	14:21	118 min	200 Hz	10 m	200 m	12

Table 3: Usable datasets.

4 H/V processing

4.1 Processing method and parameters

In order to process the H/V spectral ratios, several codes and methods were used. The classical H/V method was applied using the Geopsy `http://www.geopsy.org` software. In this method, the ratio of the smoothed Fourier Transform of selected time windows are averaged. Tukey windows (cosine taper of 5% width) of $50\,\mathrm{s}$ long overlapping by 50% were selected. Konno and Ohmachi [1998] smoothing procedure was used with a b value of 80. The classical method computed using the method of Fäh et al. [2001] was also performed.

Moreover, the time-frequency analysis method [Fäh et al., 2009] was used to estimate the ellipticity function more accurately using the Matlab code of V. Poggi. In this method, the time-frequency analysis using the Wavelet transform is computed for each component. For each frequency, the maxima over time (10 per minute with at least $0.1\,\mathrm{s}$ between each) in the TFA are determined. The Horizontal to Vertical ratio of amplitudes for each maximum is then computed and statistical properties for each frequency are derived. A Cosine wavelet with parameter 9 is used. The mean of the distribution for each frequency is stored. For the sake of comparison, the time-frequency analysis of Fäh et al. [2001], based on the spectrogram, was also used, as well as the wavelet-based TFA coded in Geopsy.

The ellipticity extraction using the Capon analysis [Poggi and Fäh, 2010] (see section on array analysis) was also performed.

Method	Freq. band	Win. length	Anti-trig.	Overlap	Smoothing
Standard H/V Geopsy	$0.2 - 20\,\mathrm{Hz}$	$50\,\mathrm{s}$	No	50%	K&O 80
Standard H/V D. Fäh	$0.2 - 20\,\mathrm{Hz}$	$30\,\mathrm{s}$	No	75%	-
H/V TFA Geopsy	$0.2 - 20\,\mathrm{Hz}$	Morlet m=8 fi=1	No	-	-
H/V TFA D. Fäh	$0.2 - 20\,\mathrm{Hz}$	Specgram	No	-	-
H/V TFA V. Poggi	$0.2 - 20\,\mathrm{Hz}$	Cosine wpar=9	No	-	No

Table 4: Methods and parameters used for the H/V processing.

4.2 Results

As remarked in the previous section, the bad recording quality of points SOZ202 and SOZ304 is affecting the H/V curve, although the peak is still visible (Fig. 3). A peak at $1.45\,\mathrm{Hz}$ in the vertical component is creating a trough at this frequency in the H/V curve, showing artificially a double peak. Moreover, this issue affects the picking precision of the peak frequency. The picked values range between 1.2 and $1.6\,\mathrm{Hz}$. Fig. 4 shows the distribution of the peak with a clear N-S gradient. Although the intermediate values are not well estimated due to the previous issue, the southern part of the covered area shows frequencies around $1.25\,\mathrm{Hz}$ (e. g. at the St Urseren church) whereas the Northern part, close to the wall of the city, shows values up to $1.5\,\mathrm{Hz}$. The results using the TFA techniques are slightly lower in frequency, but this gradient is consistent.

Moreover, all the methods to compute H/V ratios are compared at the array centre on Fig. 5, in which the classical methods were divided by $\sqrt{2}$ to correct from the Love wave contribution [Fäh et al., 2001]. The classical, TFA and FK Capon methods match well for the right flank of the peak but the peak value is slightly different for each method. The 3C FK analysis (Capon method) does not have resolution down to the peak. The peak at the SOLZ station is therefore at $1.3\,\mathrm{Hz}$, with a peak amplitude around 4 for the TFA methods.

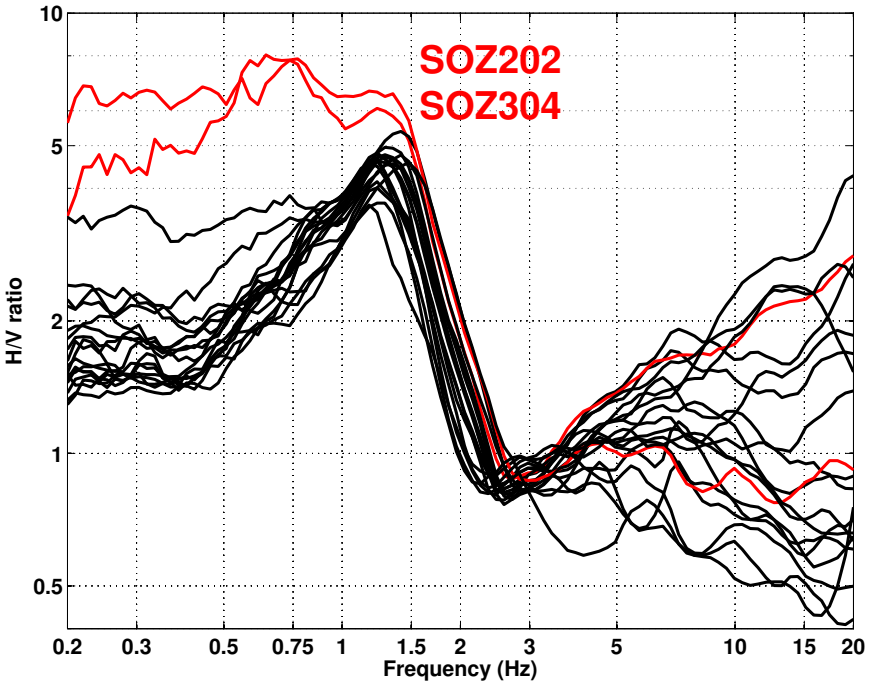

Figure 3: H/V spectral ratios (time-frequency analysis code V. Poggi).

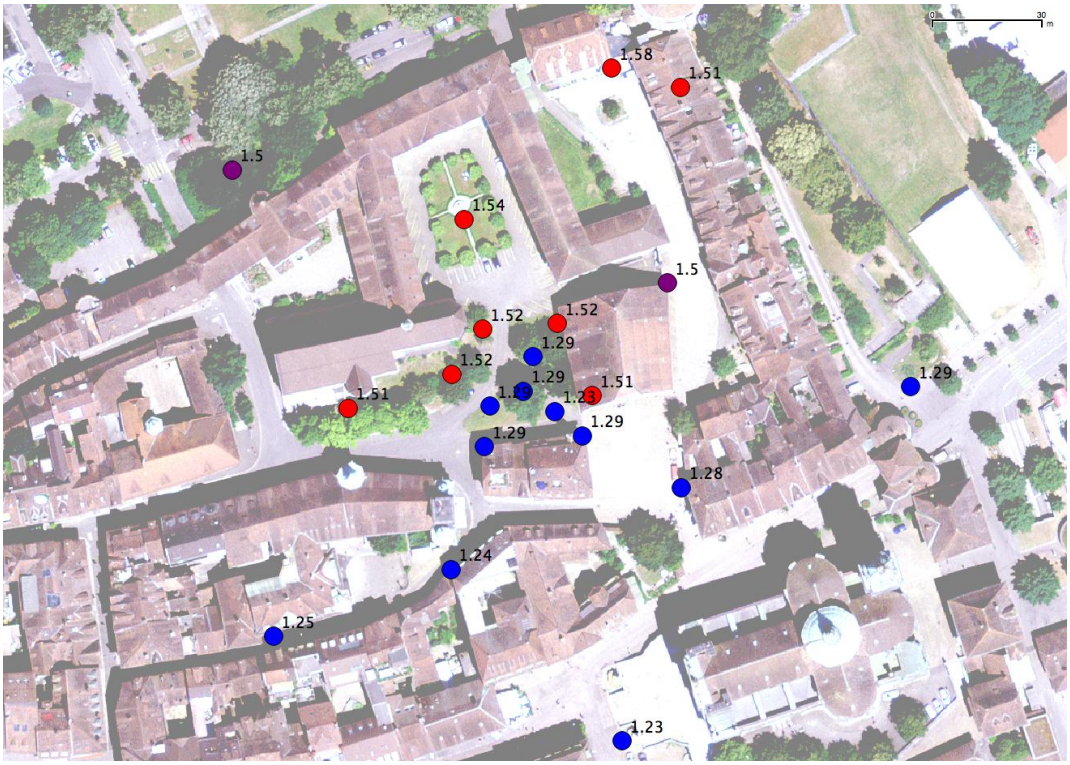

Figure 4: H/V peak frequency (in Hz) map (classical method).

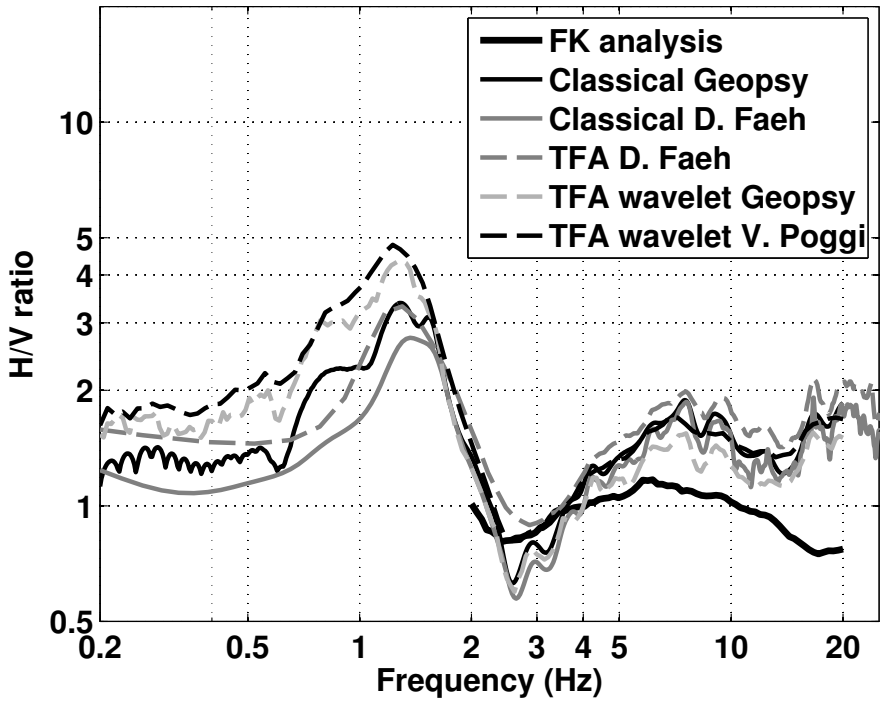

Figure 5: H/V spectral ratios for point SOZ000 using the different codes. Classical methods were divided by $\sqrt{2}$.

5 Array processing

5.1 Processing methods and parameters

The vertical components of the arrays were processed using the FK and the High-resolution FK analysis [Capon, 1969] using the Geopsy `http://www.geopsy.org` software. Better results were obtained using large time windows (300T). The results of computations of both datasets were merged to estimate the dispersion curves.

Moreover, a 3C array analysis [Fäh et al., 2008] was also performed using the array_tool_3C software [Poggi and Fäh, 2010]. It allows to derive Rayleigh and Love modes including the Rayleigh ellipticity. The results of computations of both datasets were merged to estimate the dispersion curves.

Method	Set	Freq. band	Win. length	Anti-trig.	Overlap	Grid step	Grid size	# max.
HRFK 1C	1	$1-20\,\mathrm{Hz}$	$300T$	No	50%	0.0037	2.4	5
HRFK 1C	2	$1-20\,\mathrm{Hz}$	$300T$	No	50%	0.0017	1.0	5
HRFK 3C	1	$1-20\,\mathrm{Hz}$	Wav. 10	No	50%	200	2000	5
			Tap. 0.2			m/s	m/s	
HRFK 3C	2	$1-20\,\mathrm{Hz}$	Wav. 10	No	50%	200	2000	5
			Tap. 0.2			m/s	m/s	

Table 5: Methods and parameters used for the array processing.

5.2 Obtained dispersion curves

The first mode (Rayleigh) in the 1C FK analysis could be picked between 2 and $14.5\,\mathrm{Hz}$ (Fig. 6) including its standard deviation. The velocities are ranging from $1250\,\mathrm{m/s}$ at $2\,\mathrm{Hz}$ down to $400\,\mathrm{m/s}$ at $14.5\,\mathrm{Hz}$.

Using the 3C analysis, both fundamental Rayleigh and Love modes can be picked (Fig. 6). The fundamental Rayleigh mode shows no difference with the 1C analysis (Fig. 7), except that the smoothing seems different. Rayleigh fundamental mode is picked from 2.2 to $14.5\,\mathrm{Hz}$ and Love from 1.5 to $13.4\,\mathrm{Hz}$ (Fig. 7).

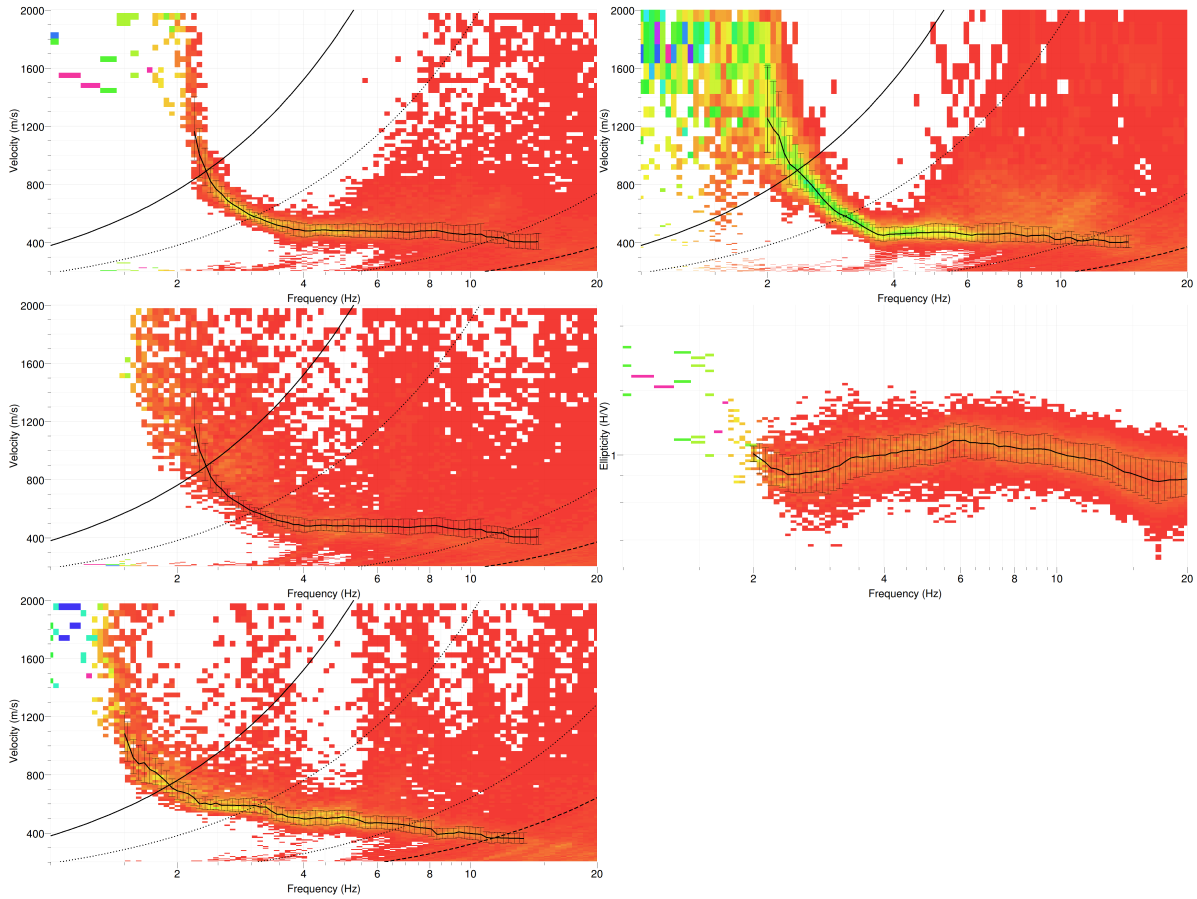

Figure 6: Dispersion curves obtained from the 3C array analysis (left) (from top to bottom: vertical, radial, transverse components), dispersion curve from the 1C analysis (top right) and ellipticity from the 3C analysis (centre right).

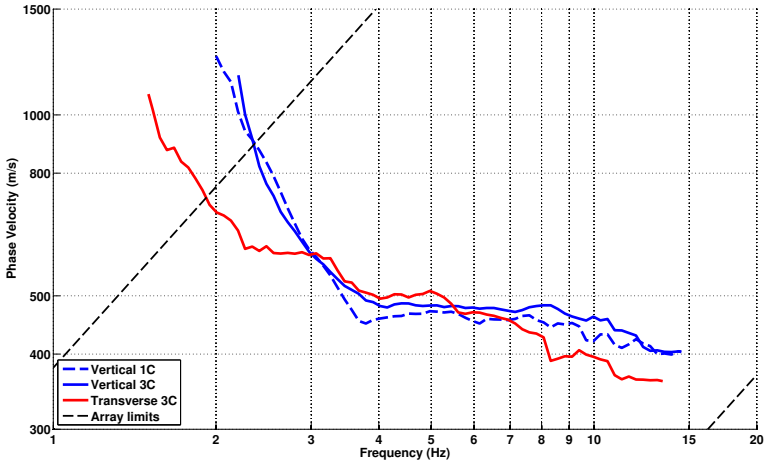

Figure 7: Picked Rayleigh and Love dispersion curves.

6 Inversion and interpretation

6.1 Inversion

For the inversion, dispersion curves of Rayleigh and Love fundamental modes, as well as the right flank of the ellipticity (TFA code V. Poggi at point SOZ101) and the ellipticity peak were used as simultaneous targets without standard deviation to avoid different weighting. The dispersion curves from the 3C FK analysis were used. A weight of 0.2 was assigned to the ellipticity curve and the ellipticity peak. After comparison of the response observed under earthquake, it happens that a fundamental frequency at higher value ($1.45\,\mathrm{Hz}$) is needed to reproduce the observed amplification. All curves were resampled using 50 points between 0.5 and $20\,\mathrm{Hz}$ in log scale.

The inversion was performed using the Improved Neighborhood Algorithm (NA) Wathelet [2008] implemented in the Dinver software. In this algorithm, the tuning parameters are the following: Ns_0 is the number of starting models, randomly distributed in the parameter space, Nr is the the number of best cells considered around these Ns_0 models, Ns is the number of new cells generated in the neighborhood of the Nr cells (Ns/Nr per cell) and It_{max} is the number of iteration of this process. The process ends with $Ns_0 + Nr * \frac{Ns}{Nr} * It_{max}$ models. The used parameters are detailed in Tab. 6.

It_{max}	Ns_0	Ns	Nr
500	10000	100	100

Table 6: Tuning parameters of Neighborhood Algorithm.

During the inversion process, low velocity zones were not allowed. The Poisson ratio was inverted in each layer in the range 0.2-0.4, up to 0.47 in the sediment part, where the water table is assumed to be localized. The density was supposed equal to $2000\,\mathrm{kg/m^3}$ except for the layer assumed to be rock ($2500\,\mathrm{kg/m^3}$). Inversions with free layer depths as well as fixed layer depths were performed. More layers than needed are used to smooth the obtained results and better explore the parameter space. 5 independent runs of 5 different parametrization schemes (5 and 6 layers over a half space and 11, 13 and 16 layers with fixed depth) were performed. For further elaborations, the best models of these 25 runs were selected (Fig. 11).

The first $10\,\mathrm{m}$ are found with increasing velocities between 250 and $400\,\mathrm{m/s}$. Below this first layer, a layer with velocities slightly increasing from 500 to $700\,\mathrm{m/s}$ down to $80\,\mathrm{m}$ depth. The lower layer has velocities between 800 and $1000\,\mathrm{m/s}$ down to $160-180\,\mathrm{m}$. At this depth an interface within the rock is responsible of the fundamental resonance frequency. The velocity of the bedrock is found around $1700\,\mathrm{m/s}$.

When comparing to the target curves (Fig. 9 and Fig. 10), all inverted targets are well represented. Ellipticity peak and curve are well reproduced.

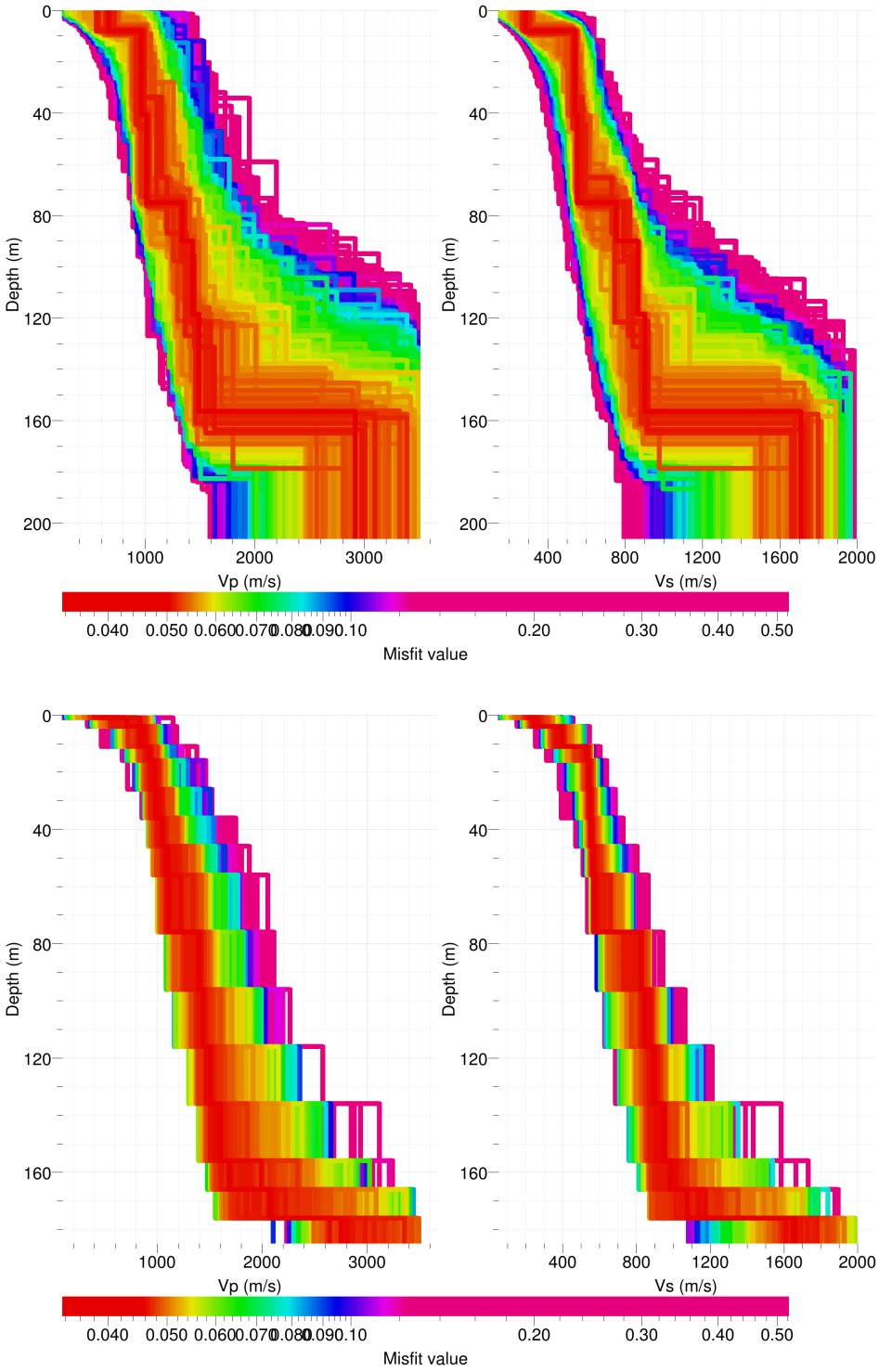

Figure 8: Inverted ground profiles in terms of V_p and V_s; top: free layer depth strategy; bottom: fixed layer depth strategy.

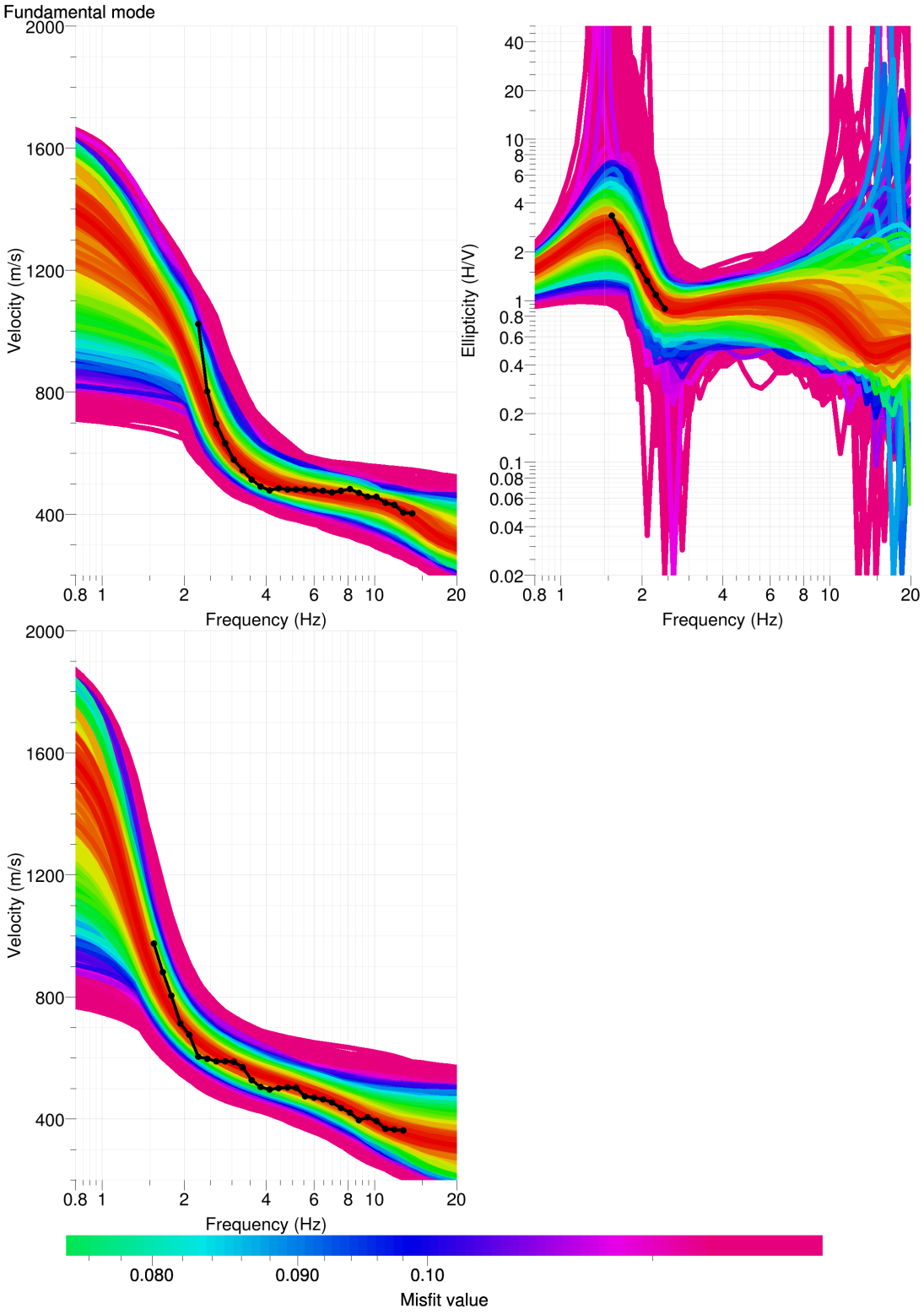

Figure 9: Comparison between inverted models and measured Rayleigh and Love modes and corresponding ellipticity, free layer depth strategy.

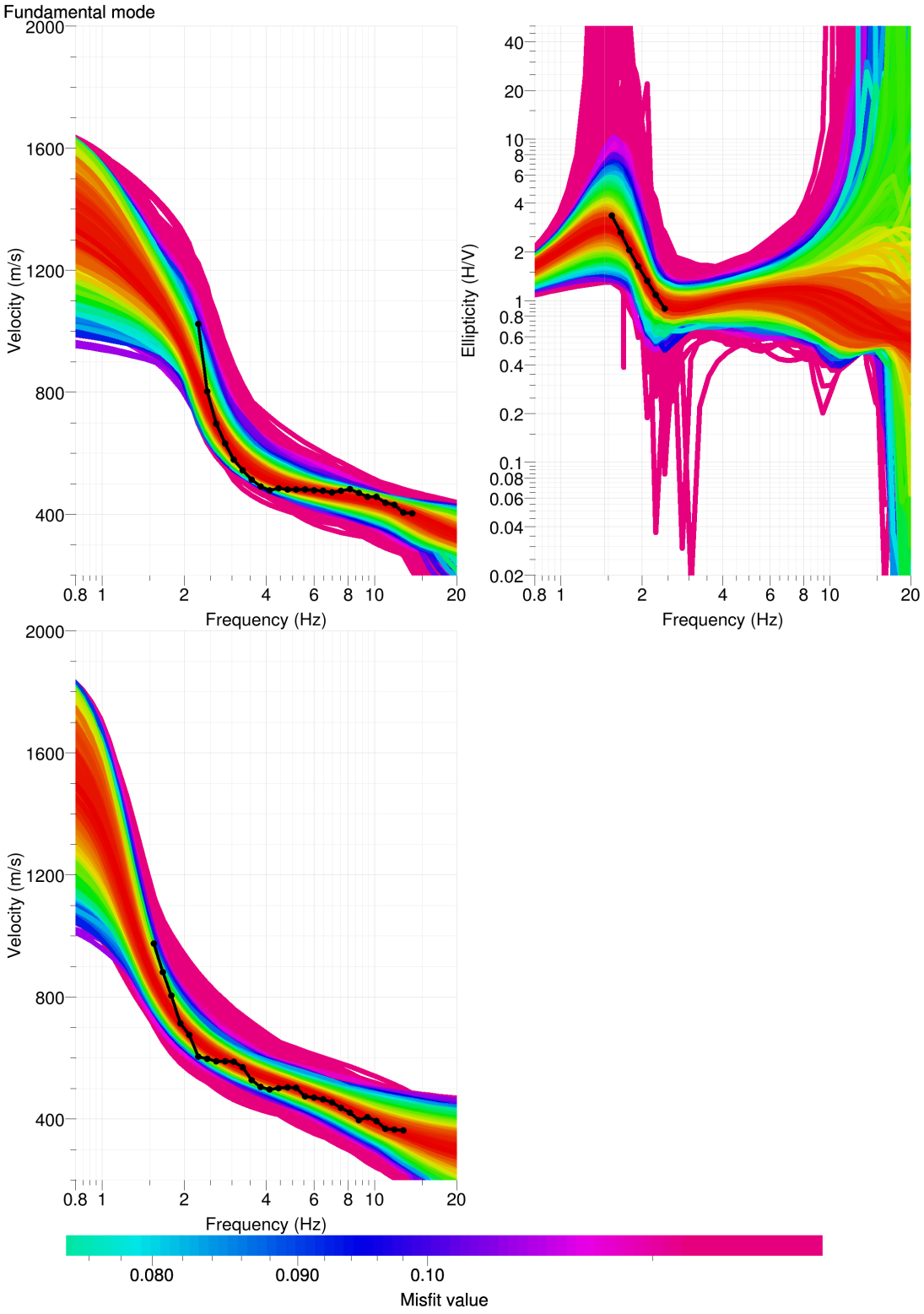

Figure 10: Comparison between inverted models and measured Rayleigh and Love modes and corresponding ellipticity, fixed layer depth strategy.

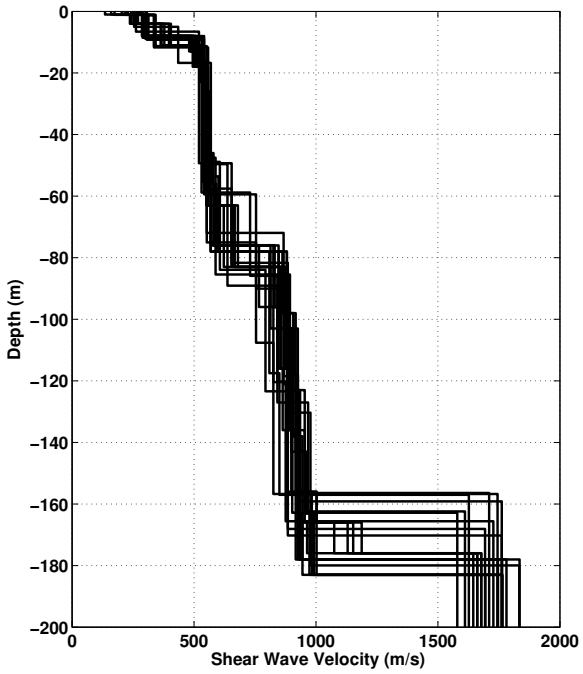

Figure 11: V_s ground profiles for the selected 25 best models.

6.2 Boreholes and interpretation

Unfortunately, no borehole is available close to the station. The closest borehole (number 1038) is located $420\,\mathrm{m}$ North (Fig. 12). It shows $36\,\mathrm{m}$ of moraine on top of the Mesozoic bedrock. At this location, the Tertiary Molasse has been washed away and the sediments lay directly on the Mesozoic limestone. This is a peculiar situation, due to a nearby fault, since at other places in Solothurn (see report on SOLB station), the Tertiary Molasse is present below the sediments. The molasse below Solothurn is USM or Lower Fresh Water Molasse made of sandstones.

The model of the quaternary sediments provided by Swisstopo (`http://www.geologieviewer.ch`) based on gravimetry anomaly seems unrealistic at this location: although the Aare basin is $160\,\mathrm{m}$ depth upstream and downstream, it is supposed to be less than $40\,\mathrm{m}$ deep below the old city of Solothurn. Boreholes 1038 ($36\,\mathrm{m}$ of moraine instead of $5\,\mathrm{m}$ in the model) and 93008 ($> 96\,\mathrm{m}$ - rock not reached - instead of $50\,\mathrm{m}$) show that the rock is located deeper than proposed in this model. This last borehole shows also $80\,\mathrm{m}$ deep lacustrine sediments, but the geology map shows that this former lake did not reach the old town of Solothurn. The reason for the mismatch with the gravimetric model is probably a wrong calibration of the model at this location where sediments are denser than downstream (lacustrine sediments).

The soil column below the station SOLZ is therefore interpreted as $10\,\mathrm{m}$ of under-consolidated moraine on top of $70\,\mathrm{m}$ of consolidated moraine. The Molasse rock is found at $80\,\mathrm{m}$ and the Mesozoïc basement, responsible for the fundamental resonance frequency, at $170\,\mathrm{m}$.

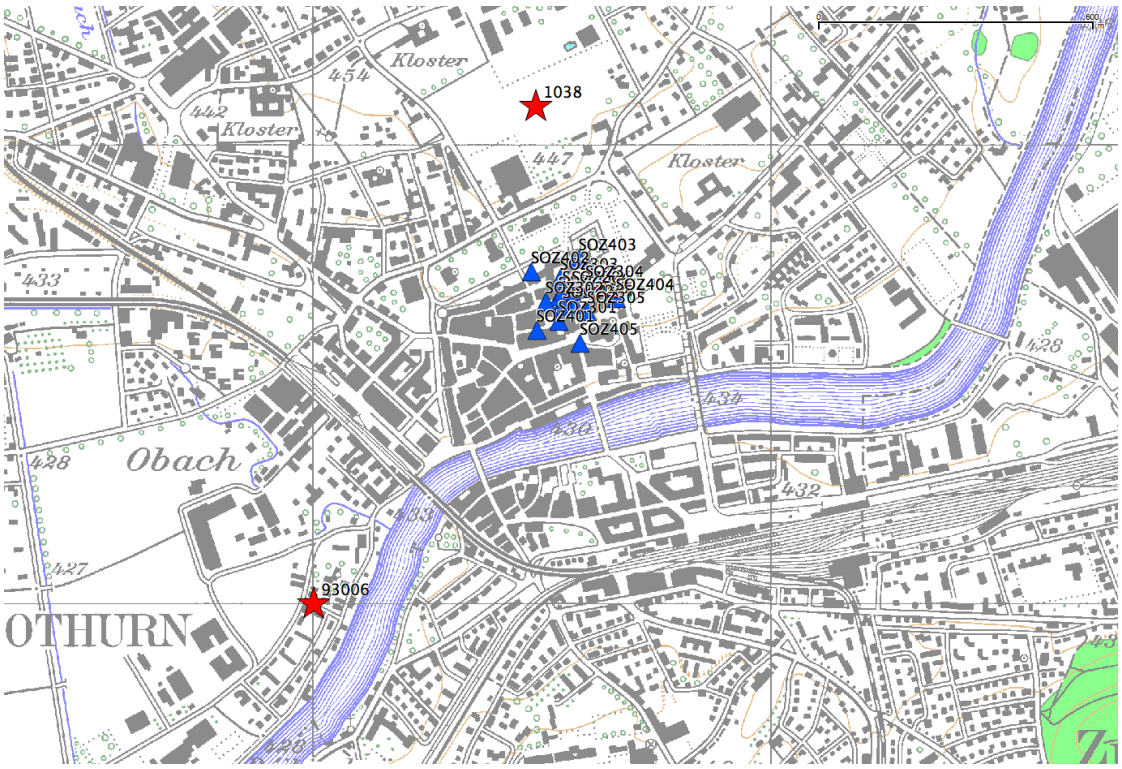

Figure 12: Map of boreholes close to the array.

6.3 Travel time average velocities and ground type

The distribution of the travel time average velocities at different depths was computed from the selected models. The uncertainty, computed as the standard deviation of the distribution of travel time average velocities for the considered models, is also provided, but its meaning is doubtful. $V_{s,30}$ is found to be $432\,\mathrm{m/s}$, meaning the site can be classified as class B in the Eurocode 8 [CEN, 2004] and in class E in SIA261 [SIA, 2003]. For SIA261, the first $10\,\mathrm{m}$ at $250 - 400\,\mathrm{m/s}$ on top of better consolidated sediments with $V_s > 500\,\mathrm{m/s}$ are characteristic of class E. Concerning EC8, the required velocity contrast for class E is larger: it needs a $V_s > 800\,\mathrm{m/s}$ below $30\,\mathrm{m}$ which is not the case here. On the official map of ground classes for SIA261 (`http://map.bafu.admin.ch`), this site is in class C. The velocity of moraine sediments was probably underestimated for the study of this map, underestimating the contrast with the surface sediments. It should be however underlined that SIA261 ground types are relatively vague and overlapping so that this kind of discrepancies is not surprising.

6.4 SH transfer function and quarter-wavelength velocity

The quarter-wavelength velocity approach [Joyner et al., 1981] provides, for a given frequency, the average velocity at a depth corresponding to 1/4 of the wavelength of interest. It is useful to identify the frequency limits of the experimental data (ellipticity peak at $1.45\,\mathrm{Hz}$ here and minimum frequency in dispersion curves at $2\,\mathrm{Hz}$). The results using this proxy show that no data is controlling the results below $90\,\mathrm{m}$, and the dispersion curves are controlling the data

	Mean (m/s)	**Uncertainty (m/s)**
$V_{s,5}$	282	20
$V_{s,10}$	315	7
$V_{s,20}$	391	6
$V_{s,30}$	432	5
$V_{s,40}$	456	5
$V_{s,50}$	473	5
$V_{s,100}$	557	5
$V_{s,150}$	637	5
$V_{s,200}$	-	-

Table 7: Travel time averages at different depths from the inverted models. Uncertainty is given as one standard deviation from the selected profiles.

down to $60\,\mathrm{m}$ (Fig. 13). Moreover, the quarter wavelength impedance-contrast introduced by Poggi et al. [2012] is also displayed in the figure. It corresponds to the ratio between two quarter-wavelength average velocities, respectively from the top and the bottom part of the velocity profile, at a given frequency [Poggi et al., 2012]. It shows a trough (inverse shows a peak) at the resonance frequency.

Moreover, the theoretical SH-wave transfer function for vertical propagation [Roesset, 1970] is computed from the inverted profiles. It is compared to the quarter-wavelength amplification [Joyner et al., 1981], that however cannot take resonances into account (Fig. 14). In this case, the models are predicting an amplification up to a factor of 3.5 at the fundamental frequency around $1.3\,\mathrm{Hz}$ as well as for upper frequencies with factors of 2.5 to 4. This will be compared to observations at this station.

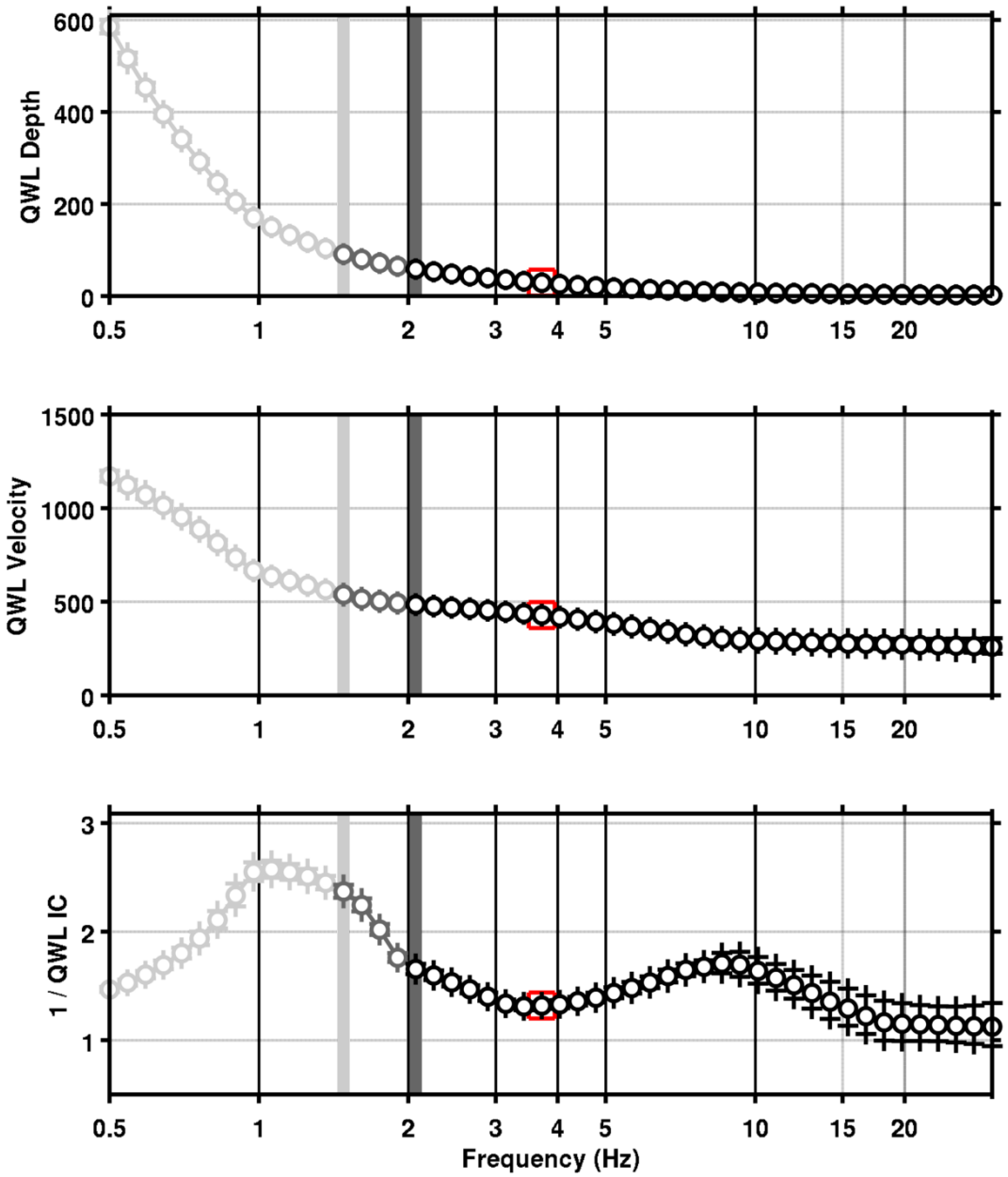

Figure 13: Quarter wavelength velocity representation of the velocity profile (top: depth, centre: velocity, bottom: inverse of the impedance contrast). Black curve is constrained by the dispersion curves, light grey is not constrained by the data. Red square is corresponding to $V_{s,30}$.

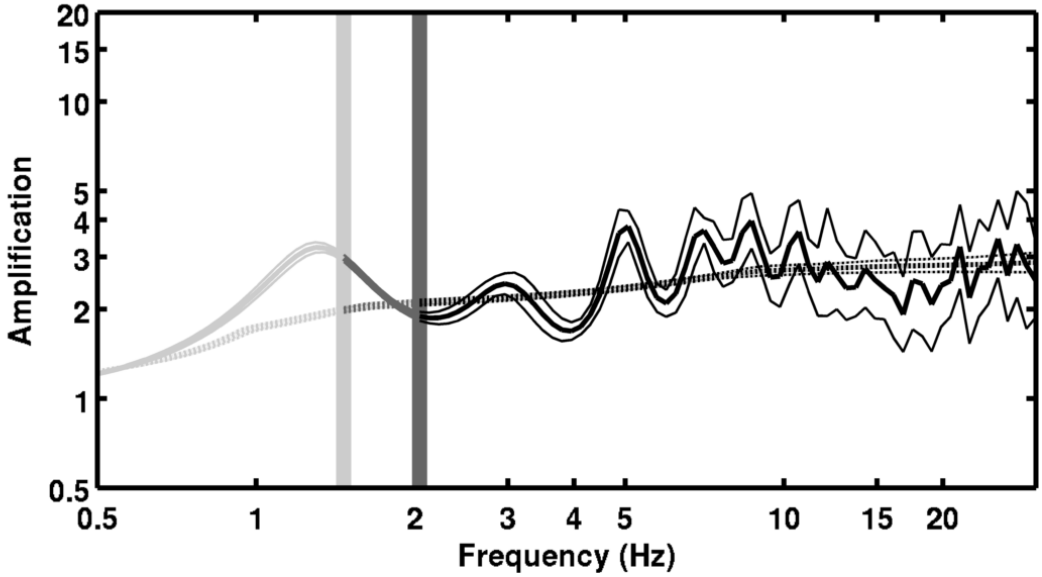

Figure 14: Theoretical SH transfer function (solid line) and quarter wavelength impedance contrast (dashed line) with their standard deviation. Significance of the greyshades is detailed in Fig. 13.

7 Conclusions

The array measurements presented in this study were successful in deriving a velocity model for the Zeughaus site in Solothurn, in the old city part, below the SOLZ station. We found a first layer of approximately $10\,\mathrm{m}$ with a relatively low velocity around $250 - 400\,\mathrm{m/s}$. A homogenous layer of moraine is then found down to $80\,\mathrm{m}$ depth with a velocity of $500 - 700\,\mathrm{m/s}$. The Molasse rock, located below, has velocities around $800 - 1000\,\mathrm{m/s}$. The interface responsible for the fundamental resonance frequency is located at $170\,\mathrm{m}$ depth. The velocity of the bedrock, that could be the Mesozoic basement is found around $1700\,\mathrm{m/s}$. $V_{s,30}$ is found to be around $430\,\mathrm{m/s}$. The ground type is B for EC8 and E for SIA261. The theoretical SH transfer function and impedance contrast of the quarter-wavelength velocity computed from the inverted profiles show large amplification up to 4 above the resonance frequency of $1.4\,\mathrm{Hz}$, with values of 2.5-4 over a broad frequency range. Recordings of the new station will allow to validate these simple models.

Acknowledgements

The authors thank Conny Hammer for the help during these measurements.

References

Sylvette Bonnefoy-Claudet, Fabrice Cotton, and Pierre-Yves Bard. The nature of noise wavefield and its applications for site effects studies. *Earth-Science Reviews*, 79(3-4): 205–227, December 2006. ISSN 00128252. doi: 10.1016/j.earscirev.2006.07.004. URL http://linkinghub.elsevier.com/retrieve/pii/S0012825206001012.

J. Capon. High-Resolution Frequency-Wavenumber Spectrum Analysis. *Proceedings of the IEEE*, 57(8):1408–1418, 1969.

CEN. *Eurocode 8: Design of structures for earthquake resistance - Part 1: General rules, seismic actions and rules for buildings*. European Committee for Standardization, en 1998-1: edition, 2004.

Donat Fäh, Fortunat Kind, and Domenico Giardini. A theoretical investigation of average H / V ratios. *Geophysical Journal International*, 145:535–549, 2001.

Donat Fäh, Gabriela Stamm, and Hans-Balder Havenith. Analysis of three-component ambient vibration array measurements. *Geophysical Journal International*, 172(1):199–213, January 2008. ISSN 0956540X. doi: 10.1111/j.1365-246X.2007.03625.x. URL http://doi.wiley.com/10.1111/j.1365-246X.2007.03625.x.

Donat Fäh, Marc Wathelet, Miriam Kristekova, Hans-Balder Havenith, Brigitte Endrun, Gabriela Stamm, Valerio Poggi, Jan Burjanek, and Cécile Cornou. Using Ellipticity Information for Site Characterisation Using Ellipticity Information for Site Characterisation. Technical report, NERIES JRA4 Task B2, 2009.

William B. Joyner, Richard E. Warrick, and Thomas E. Fumal. The effect of Quaternary alluvium on strong ground motion in the Coyote Lake, California, earthquake of 1979. *Bulletin of the Seismological Society of America*, 71(4):1333–1349, 1981.

Katsuaki Konno and Tatsuo Ohmachi. Ground-Motion Characteristics Estimated from Spectral Ratio between Horizontal and Vertical Components of Microtremor. *Bulletin of the Seismological Society of America*, 88(1):228–241, 1998.

Valerio Poggi and Donat Fäh. Estimating Rayleigh wave particle motion from three-component array analysis of ambient vibrations. *Geophysical Journal International*, 180(1):251–267, January 2010. ISSN 0956540X. doi: 10.1111/j.1365-246X.2009.04402.x. URL http://doi.wiley.com/10.1111/j.1365-246X.2009.04402.x.

Valerio Poggi, Benjamin Edwards, and Donat Fäh. Characterizing the Vertical-to-Horizontal Ratio of Ground Motion at Soft Sediment-Sites. *Bulletin of the Seismological Society of America*, 102(6), 2012. doi: 10.1785/0120120039.

J.M. Roesset. Fundamentals of soil amplification. In R. J. Hansen, editor, *Seismic Design for Nuclear Power Plants*, pages 183–244. M.I.T. Press, Cambridge, Mass., 1970. ISBN 978-0-262-08041-5. URL http://mitpress.mit.edu/catalog/item/default.asp?ttype=2\&tid=5998.

SIA. *SIA 261 Actions sur les structures porteuses*. Société suisse des ingénieurs et des architectes, Zürich, sia 261:20 edition, 2003.

Marc Wathelet. An improved neighborhood algorithm: Parameter conditions and dynamic scaling. *Geophysical Research Letters*, 35(9):1–5, May 2008. ISSN 0094-8276. doi: 10.1029/2008GL033256. URL `http://www.agu.org/pubs/crossref/2008/2008GL033256.shtml`.